Applied Materials Today 11 (2018) 13–21

Contents lists available at ScienceDirect

Applied Materials Today

journal homepage: www.elsevier.com/locate/apmt

Biocompatibility characteristics of the metal organic framework ZIF-8 for therapeutical applications

Marcus Hoop[a,*], Claudio F. Walde[a], Raffaele Riccò[c], Fajer Mushtaq[a], Anastasia Terzopoulou[a], Xiang-Zhong Chen[a], Andrew J. deMello[b], Christian J. Doonan[d], Paolo Falcaro[c,*], Bradley J. Nelson[a], Josep Puigmartí-Luis[b,*], Salvador Pané[a]

[a] Institute of Robotics and Intelligent Systems (IRIS), ETH Zurich, Tannenstrasse 3, CH-8092 Zurich, Switzerland
[b] Institute of Chemical and Bioengineering, ETH Zürich, Vladimir Prelog Weg 1, 8093 Zürich, Switzerland
[c] Institute of Physical and Theoretical Chemistry, Graz University of Technology, Stremayrgasse 9, 8010 Graz, Austria
[d] School of Chemistry and Physics, University of Adelaide, Australia, South Australia 5005, Australia

ARTICLE INFO

Article history:
Received 13 October 2017
Received in revised form
26 November 2017
Accepted 28 December 2017

Keywords:
Metal organic framework
Zeolitic imidazolate framework
ZIF-8
Zn^{2+}
Biocompatibility
Biomedical applications

ABSTRACT

Metal–organic frameworks (MOFs) are a class of crystalline materials constructed from organic linkers and inorganic nodes. MOFs typically possess ultra-high surface areas and pore volumes; thus, they are ideal candidates for biomedical applications. Zinc Imidazolate Framework 8 (ZIF-8) has been widely established in the literature as a potential candidate for on-demand drug delivery applications. Indeed, ZIF-8 has a remarkable loading capacity, stability in physiological environments, and tunable drug release properties. However, the use of ZIF-8 for *in vivo* applications requires a clear understanding of the interaction of ZIF-8 with biological tissue. In this work, we investigated the biocompatibility of ZIF-8 toward six different cell lines representing various body parts (kidney, skin, breast, blood, bones, and connective tissue). Our results suggest that ZIF-8 has no significant cytotoxicity up to a threshold value of 30 $\mu g\,mL^{-1}$. Above 30 $\mu g\,mL^{-1}$, the cytotoxicity is shown to result from the influence of released Zinc ions (Zn^{2+}) on the mitochondrial ROS production. This adverse effect is responsible for cell cycle arrest in the G2/M phase due to irreversible DNA damage, ultimately initiating cellular apoptosis pathways. Due to this insight, we encapsulated a hormone, insulin, into ZIF-8 particles and then compared its drug delivery capabilities to the aforementioned cytotoxicity values. Our results suggest that ZIF-8 is suitable for therapeutic applications. Furthermore, this study establishes a clear understanding of the interaction of ZIF-8 and its constituents with various cell lines and highlights the important biocompatibility factors that must be considered for future *in vivo* testing.

1. Introduction

Metal–organic frameworks (MOFs) are a class of porous materials that are constructed from inorganic metal ions (or clusters) coordinated to organic ligands [1]. The modular approach to MOF synthesis allows for precise control of its physical properties and chemical functionality. In particular, their highly porous nature and the potential to tune their pore size and shape, imbues MOFs with excellent drug loading capabilities. As a result they are promising candidates for drug delivery applications [2,3]. Multiple research groups have explored the use of MOFs in biomedical applications [4–8]. However, most of these studies are either limited to *ex vivo* applications or *in vitro* studies that focus solely on singular aspects of biocompatibility, *e.g.* studying a singular cell line or limiting the investigation only to one-dimensional aspects such as cell viability.

ZIF-8, constructed from 2-methylimidazole and zinc ions [9] is chemically stable in aqueous and basic media and has reported surface areas up to *ca.* 1800 $m^2\,g^{-1}$. These physical properties have been exploited for applications, such as catalysis, gas absorption and sensing techniques [10–13]. The nano-sized pore dimensions of ZIF-8 (*ca.* 11.6 Å) and pH-responsive dissolution behavior (in acidic solutions)[14,15] have motivated the investigation of ZIF-8 for biomedical applications, especially for drug delivery in cancer therapy [16,17]. Multiple research groups have successfully demonstrated the high loading capacity of ZIF-8 with small drugs and even larger biomolecules (*e.g.* bovine serum albumin (BSA) protein), within the molecular framework. Additionally, the pH

* Corresponding authors.
E-mail addresses: mhoop@ethz.ch (M. Hoop), paolo.falcaro@tugraz.at (P. Falcaro), josep.puigmarti@chem.ethz.ch (J. Puigmartí-Luis).

https://doi.org/10.1016/j.apmt.2017.12.014
2352-9407/

responsive dissolution of ZIF-8 for on-demand drug release in cancerous environment has also been reported [14,18–20]. However, the existing literature on the biocompatibility of ZIF-8 and other MOF materials is not consistent [20–25]. For example, Vasconcelos et al. did not observe significant cytotoxicity of ZIF-8 crystals loaded with an anti-cancer drug (*i.e.* doxorubicin) toward three different cell lines (NCI-H292; HT-29; HL-60) [26]. However, Horcajada et al. reported half-maximal inhibitory concentrations (IC_{50}) for ZIF-8 on HeLa and J774 cells at concentrations of 100 $\mu g\,mL^{-1}$ and 25 $\mu g\,mL^{-1}$, respectively [27]. Accordingly, a comprehensive study to understand and evaluate the biocompatible characteristics of MOFs is required, which is also essential for their therapeutic applications *in vivo*.

Biocompatibility is one of the major requirements of a material to be considered for biomedical applications [28]. Biocompatibility can be defined as the ability of a material to perform its programmed functionality (*e.g.* drug delivery inside the human body) without adversely affecting the surrounding tissue or altering homeostasis [29]. The key aspect associated with biocompatibility is the nature of the interaction between the material and human cells, and its resulting effects. Various characteristics of both inorganic and biological entities need to be carefully considered, *e.g.* surface properties, hydrophobicity, protein ad-/desorption, phagocytosis [30].

Accordingly, it is crucial to establish a comprehensive test scheme that determines the biocompatibility of the as-synthesized MOFs *in vitro* and allows for the evaluation of cell-MOF interactions before continuing their use *in vivo*. In this work, we provide a biocompatibility framework that investigates the intracellular effect of ZIF-8 on six different cell lines upon exposure to various concentrations and for different incubation time points. We identified a critical concentration of ZIF-8 for the biocompatibility of all examined cell lines, which correlated to the dissolution of zinc ions (Zn^{2+}) within the cell media. The influence of increased Zn^{2+} concentration was further studied with respect to intracellular biochemical pathways, including the generation of reactive oxygen species (ROS), the cell cycle mechanism, and apoptotic membrane disintegration. Furthermore, we identified that ZIF-8 showed significantly reduced biocompatibility characteristics above a specific particle concentration of 30 $\mu g\,mL^{-1}$, which is a fundamental finding for a future development of ZIF-8 for biomedical applications. Finally, we applied the biomimetic mineralization synthesis [31] for the encapsulation of an important biopharmaceutical, such as insulin. Falcaro and co-workers demonstrated that insulin (In) can be successfully encapsulated in ZIF-8; following the same preparation procedure the correspondent MOF bio-composite, In@ZIF-8, was biomimetically mineralized and used in this work [32]. In the current work, we demonstrated that the concentration of the encapsulated biopharmaceutical can easily be tuned, depending on the initial concentration of the guest biomolecule added to the ZIF precursors and used to trigger the biomimetic mineralization process. Given our biocompatibility findings, we conclude that ZIF-8 can be an efficient drug carrier vehicle below 30 $\mu g\,mL^{-1}$ concentrations for biomedical therapies, e.g. for the treatment of Diabetes I and II [33].

2. Materials and methods

2.1. ZIF-8 and In@ZIF-8 synthesis

ZIF-8 particles were prepared by adding a solution of 0.3 g $Zn(OAc)_2{\cdot}2H_2O$ in 5 mL of deionized (DI) water to a solution of 1.12 g of 2-methylimidazole (2-mIM) in 5 mL of DI water. The resulting solution was stirred at room-temperature overnight (*ca.* 24 h). Then, the white generated powder was centrifuged and washed 3 times with ethanol before drying at room temperature.

In@ZIF-8 samples were synthesized by mixing the appropriate amount of insulin stock solution (dissolved in a 160 mM aqueous solution of 2-mIM) with an equal volume of 40 mM aqueous stock solution of $Zn(OAc)_2{\cdot}2H_2O$. The initial concentrations of insulin were 125, 250, 500, 1000, and 2000 $\mu g\,mL^{-1}$. After addition of the zinc solution, and gentle shaking for a few seconds, the mixtures became turbid within 1 min, and was left to form ZIF-8 crystals at room temperature on a tube rotator overnight (*ca.* 16 h). Subsequently, the obtained suspension was centrifuged (4500 rpm, 5750 rcf, 20 min), the supernatant was removed (and used for UV–vis analysis of the residual insulin), and washed twice with water and twice with ethanol, centrifuging each time as above. Finally, the solids were left to dry under a fume hood at room temperature overnight. Yields were between 63 and 135 mg (41–76%) depending on the insulin concentration. For the UV–vis analysis on the solid, the In@ZIF-8 biocomposites were dissolved in 50 mM EDTA and insulin concentration was determined measuring the absorption at 278 nm (extinction coefficient: 6080 $L\,mol^{-1}\,cm^{-1}$) with a Nanodrop spectrophotometer.

2.2. Scanning electron microscopy (SEM) and X-ray diffraction (XRD) analysis

Samples for SEM and EDX were prepared by cleaning a Si wafer in acetone, isopropanol, and DI water. Afterwards, ZIF-8-based colloidal solutions were dropped on the Si substrates and dried at room temperature. SEM and EDX images were obtained employing a Zeiss Ultra 55 and Quanta 200F FEI, respectively. ZIF-8 samples for TEM were prepared on a carbon coated Cu TEM grid with a 400 mesh size. TEM images were obtained with a F30 FEI Tecnai. XRD measurements were performed on as-prepared samples and on a glass cover slip with a Bruker AXS D8 Advance equipped with a Lynxeye detector and a Cu radiation source at room temperature. The XRD data was analyzed with the X'pert Highscore software (PANalytical).

2.3. Cell culture

Human metastatic breast cancer cells (MDA-MB-231), embryonic kidney cells (HEK 293), keratinocyte (HaCaT), mouse embryonic fibroblast cells (NIH/3T3), and macrophage cells (RAW 264.7) were cultivated in DMEM cell culture medium (10% FCS, 100 × Antimycoticum) at physiological conditions. Human osteoclast cells (MG-63) were cultivated in MEM cell culture medium (10% FCS, 100 × Antimycoticum).

2.4. MTT – cell viability assay

Cells were seeded in 96-well plates at a density of 5000 cells per well in the cell medium DMEM containing 1% antibiotics and 10% FCS. After an incubation time of 4 h at 37 °C and 5% CO_2 the corresponding ZIF-8 and 2-mIM concentrations were added. Then cells were again incubated for either 72 or 120 h under the same conditions. At day 3 or 5, the MTT assays were conducted. 0.01 mL of MTT solution (15 mg of the MTT reagent, 3-(4,5-dimethylthiazol-2-yl)-2,5-diphenyl tetrazolium bromide in 3 mL of PBS at pH 7.4) was added to each well. Then the cells were incubated for 4 h, during this time, cells with an active metabolism converted the MTT reagent to a purple colored formazan crystal. These crystals were dissolved after the incubation in a 0.04 N HCl solution. Resulting purple colored solution was transferred to a new, untreated 96-well plate. Finally, the absorbance was measured on a plate reader with a test wavelength of 570 nm and a reference wavelength of 630 nm.

2.5. Atomic absorption for the measurement of Zn^{2+} concentration

ZIF-8 crystals were dissolved in three different solutions. We used 50 mM ethylenediaminetetraacetic acid (EDTA) as a chelating agent for our positive control [34]. ZIF-8 crystals were dispersed in phosphate–citrate buffers at pH 5 and 6 as well as cell medium DMEM at pH 7.4. After 5 days on a shaker at 150 rpm, the tubes were centrifuged and the supernatant was transferred into a new tube for further preparation steps. For acidification, 100 μL HCl and DI water were added to each tube in order to obtain a 1:10 or 1:50 dilution, before samples were analyzed by flame atomic absorption spectroscopy (AA240FS Varian) at a wavelength of 213.9 nm.

2.6. Reactive oxygen species (ROS) assay

To determine the amount of ROS produced by cells, the Fluorometric Intracellular ROS Kit (Sigma Aldrich) was used. Cells were seeded into a black 96-well plate at a density of 18,000 cells per well and 4 h later ZIF-8 suspension was added at concentrations ranging from 0.01 mg mL^{-1} (10 μg mL^{-1}) to 0.1 mg mL^{-1} (100 μg mL^{-1}) to a final volume of 0.1 mL. After incubation for 2 days, 0.1 mL of the ROS detection solution were added to each well. The solution contained a fluorogenic sensor, which reacts with the ROS resulting in a fluorometric product proportional to the amount of ROS present. Then, cells were again incubated for 30 min and finally the fluorescence was detected with a fluorescence multiwall plate reader at an excitation wavelength of 640 nm, and emission wavelength of 675 nm. Fluorescence images were obtained by epi-fluorescence inverted optical microscope (Olympus IX-81).

2.7. PI staining and fluorescence-activated cell sorting (FACS) for cell cycle analysis.

Cells were seeded in 6-well plates at a density of 200,000 cells per well and treated with different concentrations of ZIF-8. After an incubation time of 3 days, cells were trypsinized, centrifuged at 1000 rpm and 4 °C, followed by washing with ice-cold PBS. Then, cells were fixed with ice cold 100% ethanol, which was added dropwise while gently vortexing the pellet. Following this, cells were stored at −20 °C until the analysis was conducted. After fixation, cells were centrifuged for 5 min at 4 °C with 1500 rpm. After that, cells were again washed with cold PBS and finally resuspended in 500 μL of FACS buffer (38 mM Sodium Citrate, 69 μM PI, and 2 μL of 10 μg μL^{-1} Rnase per 500 μL of the sample). Then the solution was filtered through a cell strainer (pore diameter 50 μm) and finally the fluorescence of cells was measured by BD LSRFortesa cell analyzer with a blue (488 nm) laser.

2.8. Live/Dead cell staining

Cells were seeded at a density of 5000 cells per well in a 96-well plate. After an incubation time of 4 h ZIF-8 crystals were added at concentrations ranging from 10 to 100 μg mL^{-1}. Then the cells were incubated at 37 °C and 5% CO_2 for 3 days. Afterwards, 3 μL of the dye mixture (LIVE/DEAD BacLight; Thermofisher) was added to each well. The dye mixture consisted of 3.34 mM SYTO 9 dye and 20 mM propidium iodide combined at equal volumes. Fluorescence images were obtained by epi-fluorescence inverted optical microscope (Olympus IX-81).

3. Results and discussion

3.1. Synthesis and characterization

ZIF-8 crystals were synthesized following the one-pot synthesis method (Fig. 1a) reported by Yaghi et al. [35]. Zinc acetate ($Zn(OAc)_2$) and 2-methylimidazole (2-mIM) were both dissolved in 5 mL of deionized water and vigorously stirred. After a reaction time of 24 h, the resultant crystals were harvested and washed multiple times in ethanol followed by centrifugation. As shown in Fig. 1b and c, scanning electron microscopy (SEM) and transmission electron microscopy (TEM) images of the resulting structures indicate the formation of rhombic dodecahedral crystals with an average diameter of 1.1 μm (Fig. 1d), which corresponds to the average size of biomedically relevant ZIF-8 encapsulating biomacromolecules, as previously reported by Falcaro and co-workers [32]. As expected, energy-dispersive X-ray (EDX) spectroscopy maps confirm the presence of Zn (Fig. 1f), C (Fig. 1g), and N (Fig. 1h) elements uniformly distributed throughout each crystal. Furthermore, X-ray diffraction (XRD) measurements confirmed the characteristic peaks (7.3°, 10.4°, 12.8°, 14.8°, 16.5°, 18.1°, 22.2°, 24.6°, 25.6°, 26.7°, 29.8°, 31.5°, 32.5°) of dodecahedral ZIF-8 [36].

3.2. Influence of ZIF-8 on cell viability

In order to establish a biocompatibility framework to assess the effectiveness of ZIF-8 crystals for biomedical applications, we used six different cell lines from various tissues (see Table 1). We note that each cell line is specialized for the specific function in their organ and, hence, vary in their phenotypic pattern and consequently in their interaction with their environment [37,38].

In the first step, we assessed the influence of various ZIF-8 concentrations (0–100 μg mL^{-1}) on the cell viability and proliferation response of all six cell lines using the 'gold standard' MTT assay [39]. This assay depends on the reduction activity of intracellular, mitochondrial dehydrogenases of alive cells that converts the added tetrazolium compound into a water insoluble formazan crystal [40]. Eventually, the amount of crystal formation (determined by absorbance spectroscopy) corresponds to the viability of the present cell culture. Fig. 2a and b, shows the cell viability values of all cell lines after 72 h and 120 h, respectively. From the results, we can conclude that ZIF-8 concentrations of up to 30 μg mL^{-1} cause only a low reduction of cell viability to approximately 80% compared to the control. However, higher concentrations of ZIF-8 crystals lead to a significant cell viability drop to almost 10% for both 75 and 100 μg mL^{-1}. Furthermore, the results after 72 and 120 h show no evident variation, suggesting that the incubation time is not a pivotal factor for the reduction in cell viability.

Calculating the corresponding half-maximal inhibitory concentration, IC_{50}, and the more sensitive IC_{20} measure in Fig. 2c allowed us to assess the susceptibility of each cell line toward an increased ZIF-8 concentration. Here, the IC_{20} and IC_{50}, describe for each cell line, the critical ZIF-8 concentration that reduces cell viability by 20% and 50%, respectively. The results demonstrate that 3T3, RAW 264.7, and MG-63 cell lines show the highest sensitivity toward low ZIF-8 concentrations, with a 20% cell viability reduction at only 20–25 μg mL^{-1}. In contrast, MB-231 cancer cells displayed the highest resistance toward ZIF-8 crystals, where more than 50 μg mL^{-1} was necessary to reduce the cell viability by 20%. However, the results do not provide a comprehensive answer to the biocompatibility of ZIF-8, since the MTT assay solely assesses the cell metabolic activity and does not allow for conclusions on cell cytotoxicity. At this stage we can conclude that ZIF-8 crystals show a concentration dependent inhibition of cellular metabolism and

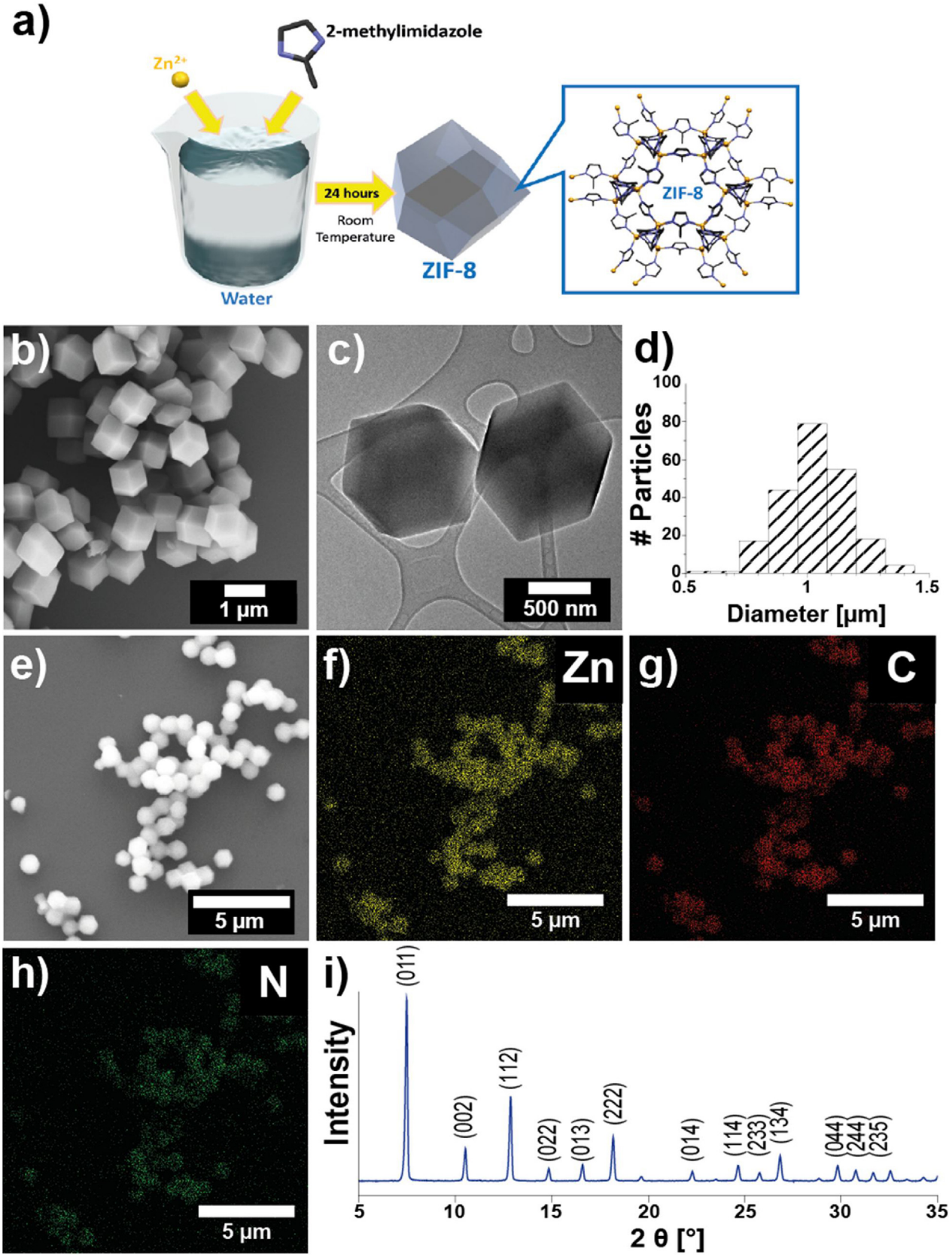

Fig. 1. (a) Reaction scheme for ZIF-8 synthesis. (b) SEM and (c) TEM images of the ZIF-8 crystals prepared together with their particle size distribution shown in (d). From (f) to (h) EDX analysis of ZIF-8 crystals shown in (e), where (f) corresponds to zinc, (g) to carbon, and (h) to nitrogen element. (i) XRD spectra with the respective peaks compared to literature [35].

Table 1
Overview of cell lines used in this study and their origin.

Cell line	Origin	Tissue	Morphology
HEK-293	Human embryo	Kidney	Epithelial
MDA-MB-231	Human	Metastatic breast	Epithelial
HaCaT	Human	Keratinocyte	Epithelial
RAW 264.7	Mouse	Ascite	Macrophage
NIH/3T3	Mouse embryo	Fibroblast	Fibroblast
MG-63	Human	Bone	Fibroblast

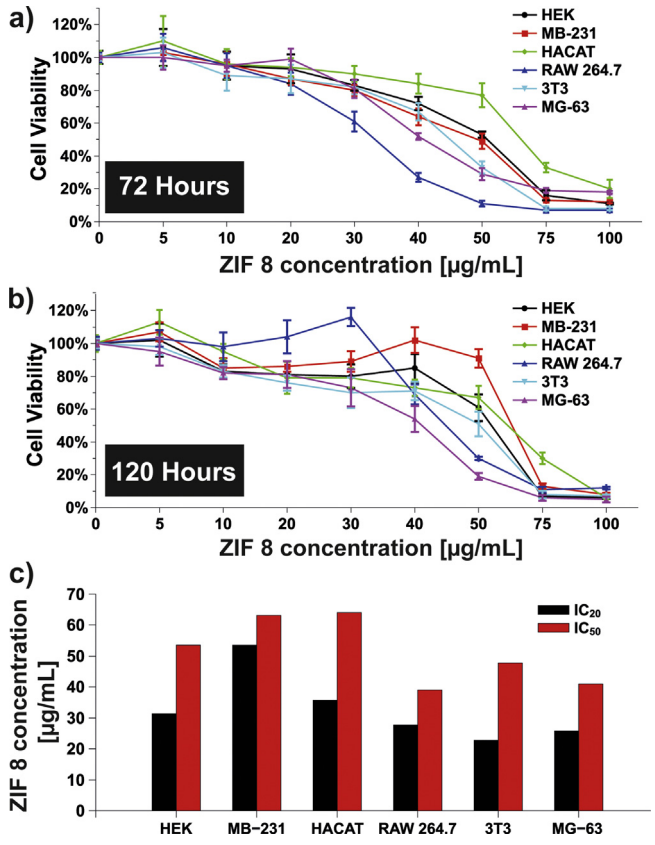

Fig. 2. MTT cell viability assay of six cell lines after (a) 72 h and (b) 120 h. (c) Calculated IC_{20} and IC_{50} values of all six cell lines ($n = 12$).

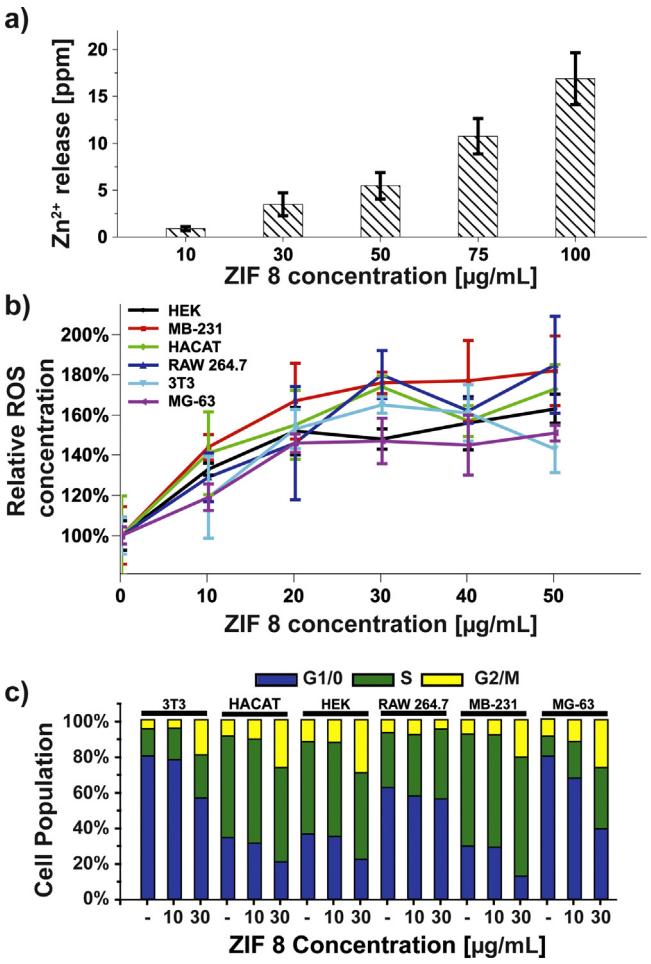

Fig. 3. (a) Amount of released zinc ions (Zn^{2+}) into the cell media at pH 7.4 after five days of incubation ($n = 5$). (b) Reactive oxygen species (ROS) generation in six cell lines after incubation with different ZIF-8 concentrations relative to a control of 0 µg mL^{-1} ZIF-8 ($n = 5$). (c) Cell cycle analysis of six cell lines after incubation with different concentrations of ZIF-8 for three days (3 independent samples with each having a final cell count of 20,000 cells).

proliferation above a critical concentration of around 30 µg mL^{-1} of pure ZIF-8.

3.3. Zn-ion release and its influence on the cell cycle

Next, we elucidated the factors accounting for the concentration dependent reduction of cell viability. In general, this could be attributed to either, or both, of the constituents of ZIF-8 crystals (Zn^{2+} or 2-mIM). The constituent 2-mIM has already been thoroughly investigated and was found to have no significant toxicological influence in *in vivo* rat studies [41]. In order to confirm these results in our test setting, we investigated the biocompatibility of 2-mIM on RAW 264.7 and 3T3 cells at various concentrations. The results shown in Fig. A1 indicate no significant influence on cell viability, even up to concentrations of 50 µg mL^{-1}. Previous studies have shown high chemical stability of ZIF-8 at neutral pH and dissolution in acidic environments [14,42]. To assess the stability of ZIF-8 crystals in cell media at physiological conditions (pH 7.4), we incubated different concentrations of ZIF-8 for 5 days and determined the release of Zn^{2+} by atomic absorption spectroscopy (AAS). Fig. 3a, shows an almost linear relationship between ZIF-8 concentration and Zn^{2+} in the supernatant. Interestingly, at a concentration of 30 µg mL^{-1} of ZIF-8 crystals, the amount of Zn^{2+} released was found to be around 3–5 µg mL^{-1}, a value that corresponds to the average homeostatic Zn^{2+} concentration reported in the literature, *i.e.* 3–6.4 µg mL^{-1} in the human blood [43,44].

Zn^{2+} ions are one of the essential trace elements responsible for multiple catalytic, structural, and regulatory functions in the human body [45,46]. Yet, increased intracellular Zn^{2+} concentrations have been shown to inhibit the Krebs cycle associated with enzymes (*e.g.* glycerol-3-phosphate dehydrogenase), induce permeability transition of the mitochondrial membrane, and inhibit the mitochondrial bc_1 cytochrome complex, leading to an augmented production and accumulation of reactive oxygen species (ROS) [47–50]. Increased ROS generation by MOFs containing other metallic nodes (*i.e.* Fe, Cr, and Al ions) has previously been reported by Yu et al. as well as Horcajada et al. [24,51]. Consequently, we expected that an increase of ZIF-8 crystals in the cell culture will increase Zn^{2+} concentration, causing an increment of intracellular ROS species due to above-mentioned effects. Hence, we measured the ROS generation in all six cell lines upon exposure to ZIF-8 concentrations between 0 and 100 µg mL^{-1} as shown in Fig. 3b. An increase in ZIF-8 up to 50 µg mL^{-1} resulted in a 50–80% increase of ROS in the cells compared to the untreated cell culture. In order to illustrate the dependency of ZIF-8 concentration and ROS production, we used the cell line with the lowest ROS generation

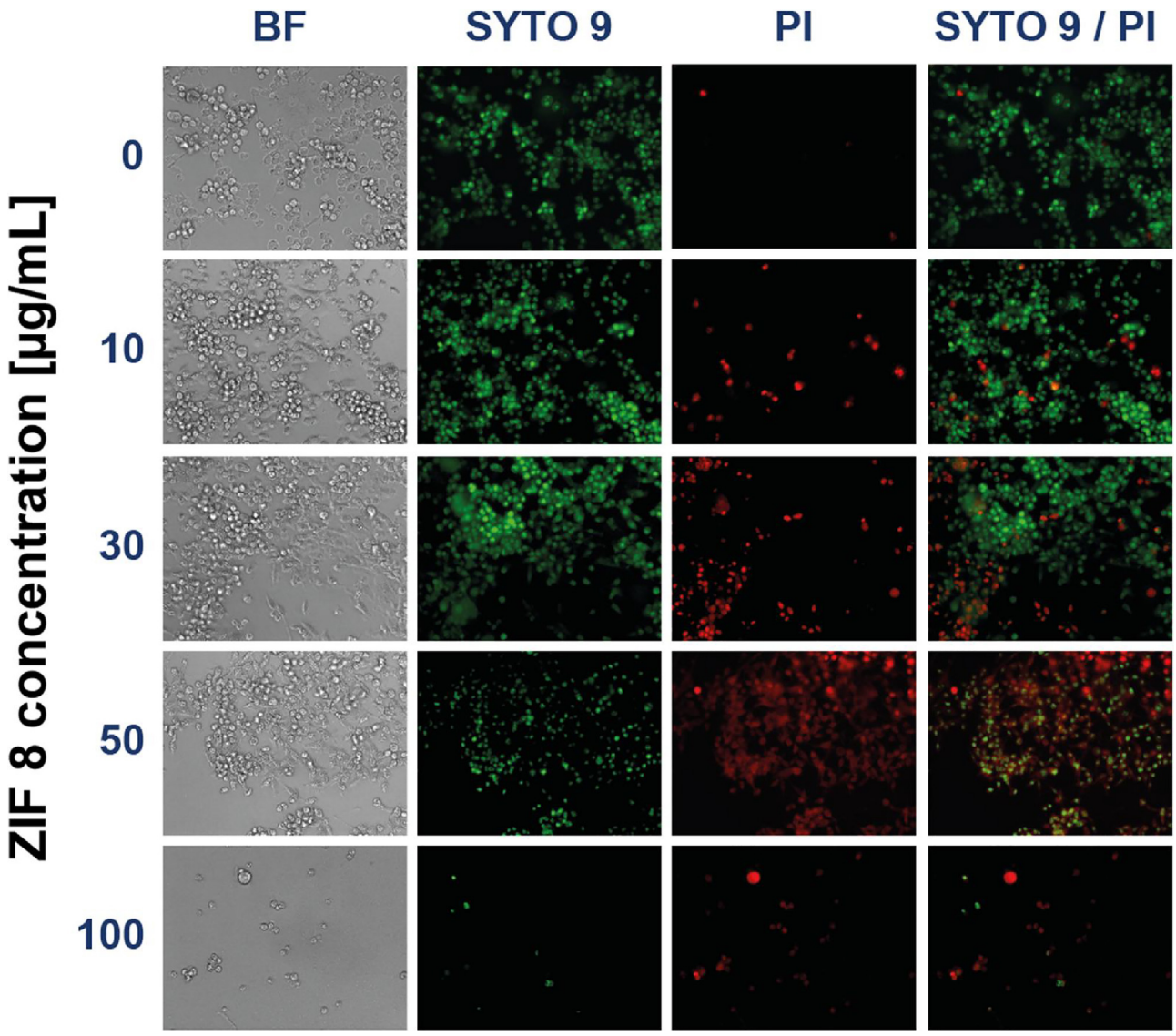

Fig. 4. Live/Dead assay of MG-63 cells after three days of incubation with different concentrations of ZIF-8: BF – Brightfield image; SYTO 9 – live cells; PI – dead cells; SYTO 9/PI – merged channel of live/dead cells.

(MG-63) and observed a significant increase in fluorescence signal, illustrating elevated ROS levels (Fig. A2). During all ROS experiments, we excluded the results from the cell cultures treated with 75 and 100 $\mu g\,mL^{-1}$, since the resulting cell density was too low to obtain a significant signal for comparison. ROS species are well known genotoxic agents causing DNA damage *via* the oxidation of DNA base pairs [52,53]. Augmented intracellular levels of ROS cause the arrest of the cell cycle at the G2/M checkpoint, a necessary step for DNA repair mechanism [54]. If ROS levels are above a certain threshold, DNA repair is no longer possible, and cellular apoptosis pathways are eventually induced [55]. Our previous results confirmed the increased ROS production upon elevated ZIF-8 concentrations. Next, we tested if the enhanced ROS concentrations influenced the cell cylce in each of the six different cell lines. After 3 days of exposure to various concentrations of ZIF-8, the cells were harvested, fixed and stained by propidium iodide (PI) [56]. The nuclear PI stain binds to the DNA and allows for DNA quantification. Here, cells in the S-phase are expected to have a higher DNA content in comparison to the G1 phase, and, subsequently, cells in the G2 phase have approximately double the amount of DNA than in G1 (see Fig. A3a). Results in Fig. 3c, provide an overview of cells exposed to ZIF-8 concentrations between 0 and 30 $\mu g\,mL^{-1}$ in the respective cell cycle stage. In all cases, no significant differences in cell cycle distribution between the control (0 $\mu g\,mL^{-1}$) and 10 $\mu g\,mL^{-1}$ ZIF-8 concentration were observed. Hence, at this concentration ZIF-8 appears to have a negligible effect on the cell cylce. However, at higher concentrations the number of cells in the G2/M phase increased significantly ($p < 0.001$) in five cell lines (except RAW 264.7), indicating the anticipated G2/M cell cycle arrest (Fig. A4).

3.4. Cytotoxicity of ZIF-8

Previous studies by Wulf et al. have shown that in case of severe DNA damage, a caspase-dependent apoptosis pathway is activated by the cells in the G2/M phase to prevent further mutagenesis [52]. This phenomenon explains the discrepancy shown for RAW 264.7 cells, where a concentration of 30 $\mu g\,mL^{-1}$ induced significant apoptosis pathways after only three days, excluding cells previously undergoing the G2/M arrest. Similar effects have been observed for all cell lines exposed to higher ZIF-8 concentrations. A majority of cells exhibited significantly reduced DNA/PI

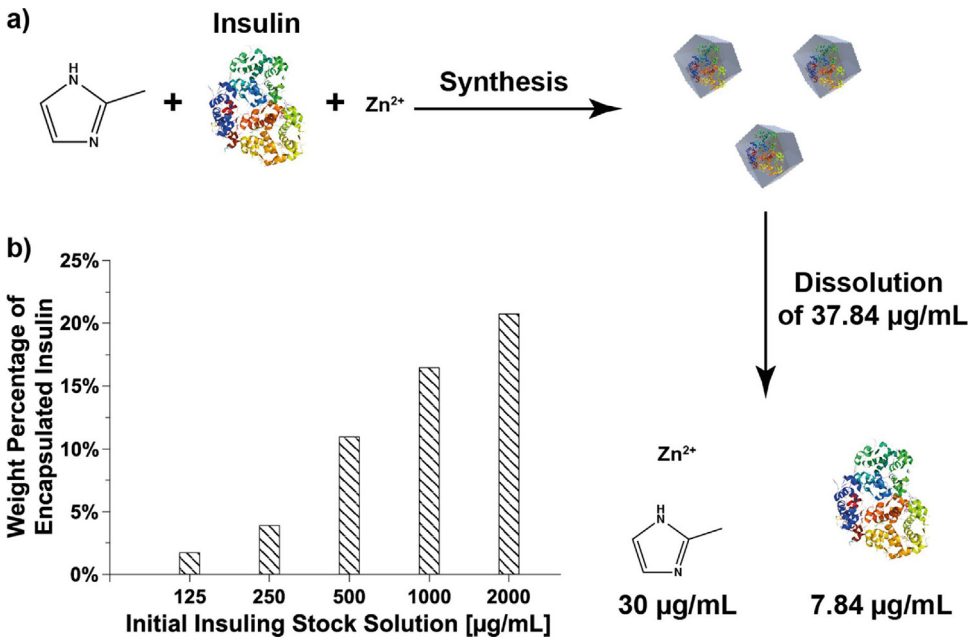

Fig. 5. (a) Schematic representation of the one-pot synthesis method for the incorporation of insulin into ZIF-8 followed by a theoretical calculation of the release of insulin from 37.84 $\mu g\,mL^{-1}$ of In@ZIF-8 (37.84 $\mu g\,mL^{-1}$ of In@ZIF-8 corresponds to 30 $\mu g\,mL^{-1}$ pure ZIF-8 crystals, which has been determined as a cytotoxic threshold value). For details concerning the calculation please refer to the appendix. (b) Initial insulin stock solutions and the resulting insulin (wt%) encapsulated into the In@ZIF-8 biocomposite.

intensity, indicating the induced apoptosis pathways (Fig. A2b and c). To validate an increased cell death in our culture, we conducted a live/dead staining assay. Commercially available dyes SYTO 9 and PI allowed us to discriminate between intact and dead (cell membrane compromised) cells. SYTO 9 is a membrane-permeable green fluorescent dye indicating alive cells, and PI is a membrane-impermeable red dye. Fig. 4 shows fluorescence microscopy image series (SYTO 9 – live; PI – dead; SYTO 9/PI – live/dead) of MG-63 cells treated with increasing ZIF-8 concentrations. From the overlay images (live/dead) it is clearly visible that an increment of ZIF-8 crystals leads to an increased amount of dead (red) cells. Above 30 $\mu g\,mL^{-1}$, fluorescence microscopy images show a reduction in cell density, which indicates an increased number of already compromised apoptotic cells.

3.5. Biomedical potential of ZIF-8

Previous literature highlighted the intriguing properties of ZIF-8 for biomedical therapies by various encapsulation strategies of biomacromolecules [32,57,58]. Here, we considered insulin as an effective therapeutic agent, because of its importance for the homeostasis of glucose. An imbalance of insulin can ultimately lead to diabetes [59]. Thus, we used a one-pot synthesis method to incorporate insulin into ZIF-8 to form In@ZIF-8 (Fig. 5a). Maximum encapsulation was achieved with an initial concentration of 2000 $\mu g\,mL^{-1}$ insulin, resulting in a loading of up to a 20.73 weight percentage (wt%). Our results demonstrate that the amount of encapsulated insulin can be varied depending on the initial insulin concentration in the reaction mixture (Fig. 5b). Conventional therapy for Type I and II diabetes requires an approximate daily dose of 0.5 IU/kg/day (1 IU of insulin = 0.035 mg) [33]. Assuming an average body weight of 70 kg, a patient would be required to administer 35 IU or 1.2 mg of insulin per day. Based upon the encapsulation efficiency of insulin in ZIF-8, a treatment of a disease such as diabetes would require *ca.* 6 mg of In@ZIF-8 in the body (*i.e.* approximately 1.2 $\mu g\,mL^{-1}$ of In@ZIF-8), which is significantly below the threshold of 30 $\mu g\,mL^{-1}$ of pure ZIF-8 (see Appendix section for detailed analysis) [60].

4. Conclusion

In this work, we propose a comprehensive framework to evaluate the biocompatibility of MOF crystals. We investigated the interaction of ZIF-8 with six different cell lines and derived a mechanism that caused cell toxicity. First, we identified a global influence of ZIF-8 concentration on cell viability. This effect was attributed to the detected release of Zn^{2+} into the cell media. Interestingly, only ZIF-8 concentrations above 30 $\mu g\,mL^{-1}$, or Zn^{2+} concentrations above 4 $\mu g\,mL^{-1}$, induced a significant reduction in cell viability. These macroscopic observations suggest an indirect, concentration dependent bio-(in)-compatibility of ZIF-8 through the release of Zn^{2+}. To verify this hypothesis, the influence of Zn^{2+} on intracellular apoptosis pathways was investigated. We confirmed that an increase in Zn^{2+} correlates with an increase in ROS generation, which leads to a cell cycle arrest in G2/M phase and ultimately activates apoptosis pathways in all investigated cell lines.

This work is highly relevant for the evaluation of suitability of MOFs as advanced biomedical devices. Our results suggest a threshold concentration for ZIF-8 of 30 $\mu g\,mL^{-1}$, which determines its biocompatibility characteristics. Low ZIF-8 concentrations (below 30 $\mu g\,mL^{-1}$), displayed biocompatible results, since the released zinc ions did not exceed homeostatic conditions. Higher concentrations of ZIF-8 had detrimental effects on the cellular metabolism and apoptotic pathways.

The high loading capability of ZIF-8, for the investigated therapeutic insulin molecule, demonstrated unique drug delivery properties of ZIF-8. Our results showed that 1.2 $\mu g\,mL^{-1}$ of In@ZIF-8 with an insulin loading of *ca.* 21% in weight is capable of delivering the necessary 0.5 IU/kg/day of insulin, sufficient for current-state of the art treatment of type I and II diabetes. Interestingly, this value is significantly below the cytotoxicity threshold of 30 $\mu g\,mL^{-1}$. Clearly, the suitability of ZIF-8 for biomedical purposes should be evaluated separately for each specific application. Future therapeutic *in vivo* trials using ZIF-8 as a drug carrier should focus on a critical concentration value significantly below 30 $\mu g\,mL^{-1}$.

Funding sources

This work was financed by the European Research Council Starting Grant "Magnetoelectric Chemonanorobotics for Chemical and Biomedical Applications (ELECTROCHEMBOTS)," by the ERC grant agreement no. 336456.

J. Puigmarti-Luis acknowledges funding from the EU through an ERC Starting Grant (ERC-2015-STG microCrysFact 677020). P. Falcaro acknowledges Graz University of Technology for the Lead Project (LP-03).

Conflict of interest

All authors confirm that there is no conflict of interest.

Acknowledgements

The authors would like to acknowledge the Scientific Center for Optical and Electron Microscopy (ScopeM) of ETH, and the FIRST laboratory for their technical support.

A. Terzopoulou would like to acknowledge the financial support from the Bodossaki Foundation.

Appendix A. Supplementary data

Supplementary data associated with this article can be found, in the online version, at doi:10.1016/j.apmt.2017.09.006.

References

[1] P. Deria, J.E. Mondloch, O. Karagiaridi, W. Bury, J.T. Hupp, O.K. Farha, Beyond post-synthesis modification: evolution of metal–organic frameworks via building block replacement, Chem. Soc. Rev. 43 (2014) 5896–5912.
[2] S. Keskin, S. Kizilel, Biomedical applications of metal organic frameworks, Ind. Eng. Chem. Res. 50 (2011) 1799–1812.
[3] R. Banerjee, H. Furukawa, D. Britt, C. Knobler, M. O'Keeffe, O.M. Yaghi, Control of pore size and functionality in isoreticular zeolitic imidazolate frameworks and their carbon dioxide selective capture properties, J. Am. Chem. Soc. 131 (2009) 3875–3877.
[4] P. Horcajada, R. Gref, T. Baati, P.K. Allan, G. Maurin, P. Couvreur, G. Ferey, R.E. Morris, C. Serre, Metal–organic frameworks in biomedicine, Chem. Rev. 112 (2012) 1232–1268.
[5] R. Liu, T. Yu, Z. Shi, Z.Y. Wang, The preparation of metal–organic frameworks and their biomedical application, Int. J. Nanomed. 11 (2016) 1187–1200.
[6] K.D. Lu, C.B. He, N.N. Guo, C. Chan, K.Y. Ni, R.R. Weichselbaum, W.B. Lin, Chlorin-based nanoscale metal–organic framework systemically rejects colorectal cancers via synergistic photodynamic therapy and checkpoint blockade immunotherapy, J. Am. Chem. Soc. 138 (2016) 12502–12510.
[7] J.J. Liu, Y. Yang, W.W. Zhu, X. Yi, Z.L. Dong, X.N. Xu, M.W. Chen, K. Yang, G. Lu, L.X. Jiang, Z. Liu, Nanoscale metal–organic frameworks for combined photodynamic & radiation therapy in cancer treatment, Biomaterials 97 (2016) 1–9.
[8] X.G. Wang, Z.Y. Dong, H. Cheng, S.S. Wan, W.H. Chen, M.Z. Zou, J.W. Huo, H.X. Deng, X.Z. Zhang, A multifunctional metal–organic framework based tumor targeting drug delivery system for cancer therapy, Nanoscale 7 (2015) 16061–16070.
[9] J.B. James, Y.S. Lin, Kinetics of ZIF-8 thermal decomposition in inert, oxidizing, and reducing environments, J. Phys. Chem. C 120 (2016) 14015–14026.
[10] S. Van Cleuvenbergen, I. Stassen, E. Gobechiya, Y.X. Zhang, K. Markey, D.E. De Vos, C. Kirschhock, B. Champagne, T. Verbiest, M.A. van der Veen, ZIF-8 as nonlinear optical material: influence of structure and synthesis, Chem. Mater. 28 (2016) 3203–3209.
[11] C.M. Miralda, E.E. Macias, M.Q. Zhu, P. Ratnasamy, M.A. Carreon, Zeolitic imidazole framework-8 catalysts in the conversion of CO_2 to chloropropene carbonate, ACS Catal. 2 (2012) 180–183.
[12] H.L. Huang, W.J. Zhang, D.H. Liu, B. Liu, G.J. Chen, C.L. Zhong, Effect of temperature on gas adsorption and separation in ZIF-8: a combined experimental and molecular simulation study, Chem. Eng. Sci. 66 (2011) 6297–6305.
[13] G. Lu, J.T. Hupp, Metal–organic frameworks as sensors: a ZIF-8 based Fabry-Perot device as a selective sensor for chemical vapors and gases, J. Am. Chem. Soc. 132 (2010) 7832–7833.
[14] C.Y. Sun, C. Qin, X.L. Wang, G.S. Yang, K.Z. Shao, Y.Q. Lan, Z.M. Su, P. Huang, C.G. Wang, E.B. Wang, Zeolitic imidazolate framework-8 as efficient pH-sensitive drug delivery vehicle, Dalton Trans. 41 (2012) 6906–6909.
[15] D. Fairen-Jimenez, S.A. Moggach, M.T. Wharmby, P.A. Wright, S. Parsons, T. Duren, Opening the gate: framework flexibility in ZIF-8 explored by experiments and simulations, J. Am. Chem. Soc. 133 (2011) 8900–8902.
[16] M. Zheng, S. Liu, X.G. Guan, Z.G. Xie, One-step synthesis of nanoscale zeolitic imidazolate frameworks with high curcumin loading for treatment of cervical cancer, ACS Appl. Mater. Inter. 7 (2015) 22181–22187.
[17] N.A.H.M. Nordin, A.F. Ismail, A. Mustafa, R.S. Murali, T. Matsuura, The impact of ZIF-8 particle size and heat treatment on CO_2/CH_4 separation using asymmetric mixed matrix membrane, RSC Adv. 4 (2014) 52530–52541.
[18] H.Q. Zheng, Y.N. Zhang, L.F. Liu, W. Wan, P. Guo, A.M. Nystrom, X.D. Zou, One-pot synthesis of metal organic frameworks with encapsulated target molecules and their applications for controlled drug delivery, J. Am. Chem. Soc. 138 (2016) 962–968.
[19] P. Kumar, V. Bansal, A.K. Paul, L.M. Bharadwaj, A. Deep, K.H. Kim, Biological applications of zinc imidazole framework through protein encapsulation, Appl. Nanosci. 6 (2016) 951–957.
[20] H.Z. Yu, X.Y. Qiu, P. Neelakanda, L. Deng, N.M. Khashab, S.P. Nunes, K.V. Peinemann, Hollow ZIF-8 nanoworms from block copolymer templates, Sci. Rep. -Uk. 5 (2015) 15275.
[21] E. Shearier, P.F. Cheng, Z.A. Zhu, J.M. Bao, Y.H. Hu, F. Zhao, Surface defection reduces cytotoxicity of Zn(2-methylimidazole)(2) (ZIF-8) without compromising its drug delivery capacity, RSC Adv. 6 (2016) 4128–4135.
[22] J. Zhuang, C.H. Kuo, L.Y. Chou, D.Y. Liu, E. Weerapana, C.K. Tsung, Optimized metal–organic-framework nanospheres for drug delivery: evaluation of small-molecule encapsulation, ACS Nano 8 (2014) 2812–2819.
[23] A. Ruyra, A. Yazdi, J. Espin, A. Carne-Sanchez, N. Roher, J. Lorenzo, I. Imaz, D. Maspoch, Synthesis, culture medium stability, and in vitro and in vivo zebrafish embryo toxicity of metal–organic framework nanoparticles, Chem. -Eur. J. 21 (2015) 2508–2518.
[24] R. Grall, T. Hidalgo, J. Delic, A. Garcia-Marquez, S. Chevillard, P. Horcajada, In vitro biocompatibility of mesoporous metal (III; Fe, Al, Cr) trimesate MOF nanocarriers, J. Mater. Chem. B 3 (2015) 8279–8292.
[25] M. Sajid, Toxicity of nanoscale metal organic frameworks: a perspective, Environ. Sci. Pollut. Res. Int. 23 (2016) 14805–14807.
[26] I.B. Vasconcelos, T.G. da Silva, G.C.G. Militao, T.A. Soares, N.M. Rodrigues, M.O. Rodrigues, N.B. da Costa, R.O. Freire, S.A. Junior, Cytotoxicity and slow release of the anti-cancer drug doxorubicin from ZIF-8, RSC Adv. 2 (2012) 9437–9442.
[27] C. Tamames-Tabar, D. Cunha, E. Imbuluzqueta, F. Ragon, C. Serre, M.J. Blanco-Prieto, P. Horcajada, Cytotoxicity of nanoscaled metal–organic frameworks, J. Mater. Chem. B 2 (2014) 262–271.
[28] C. Wiegand, U.C. Hipler, Methods for the measurement of cell and tissue compatibility including tissue regeneration processes, GMS Krankenhaushy. Interdiszipl. 3 (2008) Doc12.
[29] D.F. Williams, On the mechanisms of biocompatibility, Biomaterials 29 (2008) 2941–2953.
[30] Y. Yoshioka, K. Higashisaka, Y. Tsutsumi, Biocompatibility of nanomaterials, in: L. Zheng-Rong, S. Shinji (Eds.), Nanomaterials in Pharmacology, Springer, New York, Heidelberg, Dordrecht, London, 2016, pp. 185–199.
[31] C. Doonan, R. Ricco, K. Liang, D. Bradshaw, P. Falcaro, Metal–organic frameworks at the biointerface: synthetic strategies and applications, Acc. Chem. Res. 6 (2017) 1423–1432.
[32] K. Liang, R. Ricco, C.M. Doherty, M.J. Styles, S. Bell, N. Kirby, S. Mudie, D. Haylock, A.J. Hill, C.J. Doonan, P. Falcaro, Biomimetic mineralization of metal–organic frameworks as protective coatings for biomacromolecules, Nat. Commun. 6 (2015) 7240.
[33] V. Fonseca, Diabetes: Improving Patient Care, Oxford University Press, 2010.
[34] X.L. Wang, J.F. Shi, S.H. Zhang, H. Wu, Z.Y. Jiang, C. Yang, Y.X. Wang, L. Tang, A.F. Yan, MOF-templated rough, ultrathin inorganic microcapsules for enzyme immobilization, J. Mater. Chem. B 3 (2015) 6587–6598.
[35] K.S. Park, Z. Ni, A.P. Cote, J.Y. Choi, R.D. Huang, F.J. Uribe-Romo, H.K. Chae, M. O'Keeffe, O.M. Yaghi, Exceptional chemical and thermal stability of zeolitic imidazolate frameworks, Proc. Natl. Acad. Sci. U. S. A. 103 (2006) 10186–10191.
[36] A.F. Gross, E. Sherman, J.J. Vajo, Aqueous room temperature synthesis of cobalt and zinc sodalite zeolitic imidizolate frameworks, Dalton Trans. 41 (2012) 5458–5460.
[37] D. Arendt, J.M. Musser, C.V.H. Baker, A. Bergman, C. Cepko, D.H. Erwin, M. Pavlicev, G. Schlosser, S. Widder, M.D. Laubichler, G.P. Wagner, The origin and evolution of cell types, Nat. Rev. Genet. 17 (2016) 744–757.
[38] D. Arendt, The evolution of cell types in animals: emerging principles from molecular studies, Nat. Rev. Genet. 9 (2008) 868–882.
[39] A. van Tonder, A.M. Joubert, A.D. Cromarty, Limitations of the 3-(4, 5-dimethylthiazol-2-yl)-2,5-diphenyl-2H-tetrazolium bromide (MTT) assay when compared to three commonly used cell enumeration assays, BMC Res. Notes 8 (2015) 47.
[40] T.L. Riss, R.A. Moravec, A.L. Niles, S. Duellman, H.A. Benink, T.J. Worzella, L. Minor, Cell viability assays, in: G.S. Sittampalam, N.P. Coussens, K. Brimacombe, A. Grossman, M. Arkin, D. Auld, et al. (Eds.), Assay Guidance Manual. Bethesda, MD, 2004.
[41] J.D. Johnson, D. Reichelderfer, A. Zutshi, S. Graves, D. Walters, C. Smith, Toxicokinetics of 2-methylimidazole in male and female F344 rats, J. Toxicol. Environ. Health A 65 (2002) 869–879.
[42] S.H. Pang, C. Han, D.S. Sholl, C.W. Jones, R.P. Lively, Facet-specific stability of ZIF-8 in the presence of acid gases dissolved in aqueous solutions, Chem. Mater. 28 (2016) 6960–6967.
[43] W.B. Herring, B.S. Leavell, L.M. Paixo, J.H. Yoe, Trace metals in human plasma and red blood cells. A study of magnesium, chromium, nickel, copper and

zinc. I. Observations of normal subjects, Am. J. Clin. Nutr. 8 (1960) 846–854.
[44] G. Lusvardi, G. Malavasi, L. Menabue, M.C. Menziani, A. Pedone, U. Segre, V. Aina, A. Perardi, C. Morterra, F. Boccafoschi, S. Gatti, M. Bosetti, M. Cannas, Properties of zinc releasing surfaces for clinical applications, J. Biomater. Appl. 22 (2008) 505–526.
[45] N. Roohani, R. Hurrell, R. Kelishadi, R. Schulin, Zinc and its importance for human health: an integrative review, J. Res. Med. Sci. 18 (2013) 144–157.
[46] H. Tapiero, K.D. Tew, Trace elements in human physiology and pathology: zinc and metallothioneins, Biomed. Pharmacother. 57 (2003) 399–411.
[47] A. Clausen, T. McClanahan, S.G. Ji, J.H. Weiss, Mechanisms of rapid reactive oxygen species generation in response to cytosolic Ca^{2+} or Zn^{2+} loads in cortical neurons, PLOS ONE 8 (2013) e83347.
[48] K.E. Dineley, T.V. Votyakova, I.J. Reynolds, Zinc inhibition of cellular energy production: implications for mitochondria and neurodegeneration, J. Neurochem. 85 (2003) 563–570.
[49] L.J. Martin, N.A. Adams, Y. Pan, A. Price, M. Wong, The mitochondrial permeability transition pore regulates nitric oxide-mediated apoptosis of neurons induced by target deprivation, J. Neurosci. 31 (2011) 359–370.
[50] T.A. Link, G. von Jagow, Zinc ions inhibit the QP center of bovine heart mitochondrial bc1 complex by blocking a protonatable group, J. Biol. Chem. 270 (1995) 25001–25006.
[51] K. Liu, Y. Gao, J. Liu, Y. Wen, Y. Zhao, K. Zhang, G. Yu, Photoreactivity of metal–organic frameworks in aqueous solutions: metal dependence of reactive oxygen species production, Environ. Sci. Technol. 50 (2016) 3634–3640.
[52] T. Thorn, R. Gniadecki, A.B. Petersen, J. Vicanova, H.C. Wulf, Differences in activation of G2/M checkpoint in keratinocytes after genotoxic stress induced by hydrogen peroxide and ultraviolet A radiation, Free Radic. Res. 35 (2001) 405–416.
[53] M.S. Cooke, M.D. Evans, M. Dizdaroglu, J. Lunec, Oxidative DNA damage: mechanisms, mutation, and disease, FASEB J. 17 (2003) 1195–1214.
[54] J. Cadet, J.R. Wagner, DNA base damage by reactive oxygen species, oxidizing agents, and UV radiation, Cold Spring Harb. Perspect. Biol. 5 (2013).
[55] K.F. Hua, P.C. Liao, Z. Fang, F.L. Yang, Y.L. Yang, Y.L. Chen, Y.C. Chiu, M.L. Liu, Y. Lam, S.H. Wu, Generation of reactive oxygen species by polyenylpyrroles derivatives causes DNA damage leading to G2/M arrest and apoptosis in human oral squamous cell carcinoma cells, PLOS ONE 8 (2013) e67603.
[56] K.H. Kim, J.M. Sederstrom, Assaying cell cycle status using flow cytometry, Curr. Protoc. Mol. Biol. 111 (2015) 2861.
[57] N. Liedana, A. Galve, C. Rubio, C. Tellez, J. Coronas, Caf@Zif-8: one-step encapsulation of caffeine in mof, ACS Appl. Mater. Inter. 4 (2012) 5016–5021.
[58] M.B. Majewski, A.J. Howarth, P. Li, M.R. Wasielewski, J.T. Hupp, O.K. Farha, Enzyme encapsulation in metal–organic frameworks for applications in catalysis, Cryst. Eng. Commun. 19 (2017) 4082–4091.
[59] A.C. Maritim, R.A. Sanders, J.B. Watkins, Diabetes, oxidative stress, and antioxidants: a review, J. Biochem. Mol. Toxic. 17 (2003) 24–38.
[60] K.P. Davy, D.R. Seals, Total blood volume in healthy young and older men, J. Appl. Physiol. 76 (1994) 2059–2062.